MOLECULAR BIOLOGY

TSC22D4 interacts with Akt1 to regulate glucose metabolism

Sevgican Demir[1,2,3], Gretchen Wolff[1,2,3], Annika Wieder[1,2,3], Adriano Maida[1,2,3], Lea Bühler[1,2,3], Maik Brune[1,2,3], Oksana Hautzinger[1,2,3], Annette Feuchtinger[4], Tanja Poth[5], Julia Szendroedi[1,2,3], Stephan Herzig[1,2,3], Bilgen Ekim Üstünel[1,2,3]*

Maladaptive insulin signaling is a key feature in the pathogenesis of severe metabolic disorders, including obesity and diabetes. Enhancing insulin sensitivity represents a major goal in the treatment of patients affected by diabetes. Here, we identify transforming growth factor–β1 stimulated clone 22 D4 (TSC22D4) as a novel interaction partner for protein kinase B/Akt1, a critical mediator of insulin/phosphatidylinositol 3-kinase signaling pathway. While energy deprivation and oxidative stress promote the TSC22D4-Akt1 interaction, refeeding mice or exposing cells to glucose and insulin impairs this interaction, which relies on an intrinsically disordered region (D2 domain) within TSC22D4. Functionally, the interaction with TSC22D4 reduces basal phosphorylation of Akt and its downstream targets during starvation, thereby promoting insulin sensitivity. Genetic, liver-specific reconstitution experiments in mice demonstrate that the interaction between TSC22D4 and Akt1 improves glucose handling and insulin sensitivity. Overall, our findings postulate a model whereby TSC22D4 acts as an environmental sensor and interacts with Akt1 to regulate insulin signaling and glucose metabolism.

INTRODUCTION

Insulin signaling is an evolutionarily conserved pathway that is central to the regulation of cell growth, cell proliferation, development, longevity, and glucose and lipid metabolism. When insulin binds to the insulin receptor (IR), IR gets activated and phosphorylates IR substrate (IRS) to initiate a cascade of phosphorylation events, leading to the activation of protein kinase B (PKB)/Akt (*1*). Once phosphorylated by phosphatidylinositol 3-kinase–dependent kinase 1 (PDK1) and mechanistic target of rapamycin complex 2 (mTORC2) on T308 and S473, respectively, Akt kinase becomes catalytically active and phosphorylates a wide range of targets including glycogen synthase kinase 3β (GSK3β), forkhead box O1 (FoxO1), and tuberous sclerosis complex 2 (TSC2) to promote cell survival, cell growth, and cell proliferation as well as to regulate glucose and lipid metabolism (*2*). In addition to the phosphorylation events, protein-protein interactions play a key role in regulating Akt function (*3*). C-jun N-terminal kinase (JNK)–interacting protein 1 (JIP1), growth factor receptor–binding protein 10 (Grb10), and tribbles homolog 3 (Trb3) represent only a few of the proteins that interact with Akt to regulate its distinct functions (*3*–*5*).

Elevated insulin levels during overnutrition initiate negative feedback loops in insulin signaling pathway, leading to the pathological condition known as insulin resistance, in which metabolic organs fail to respond to circulating insulin levels. Overnutrition also induces a chronic low-grade inflammation that activates JNK and inhibits adenosine monophosphate (AMP)–activated protein kinase (AMPK), contributing to insulin resistance, which may further progress into type 2 diabetes, which is hardly reversible and leads to several complications in peripheral organs in the long run (*6*).

Recently, we identified transforming growth factor–β1 (TGFβ1) stimulated clone 22 D4 (TSC22D4) as a regulator of Akt signaling pathway in mouse models of type 2 diabetes (*7*). TSC22D4 belongs to the TSC22 protein family, which contains the evolutionarily conserved TSC box with a leucine zipper motif. TSC22 family consists of four proteins, such as TSC22D1, TSC22D2, TSC22D3, and TSC22D4 with alternatively spliced isoforms, and they can homo- and heterodimerize with each other to regulate cell biological functions such as cellular senescence, cell proliferation, and apoptosis (*8*–*13*).

Despite being found two decades ago, our current knowledge of the regulation and function of TSC22D4 remains very limited. TSC22D4 expression increases in cultured kidney cells upon osmotic stress, and TSC22D4 subcellular localization in neurons alters during stages of embryonic development and differentiation (*10*, *13*). TSC22D4 also suppresses cellular senescence by impairing junB function (*14*). Previously, we have shown that hepatic TSC22D4 expression increases upon liver damage and cancer cachexia and reprograms liver lipid metabolism (*15*). Targeting TSC22D4 expression in the livers of mice with type 2 diabetes alleviates insulin resistance and hyperglycemia (*7*). Notably, in obese human patients, elevated TSC22D4 expression in the liver positively correlates with insulin resistance (*7*). These studies establish a novel and reciprocal connection between TSC22D4 and metabolic regulation, yet the molecular mechanism of this connection remains largely elusive.

Here, we identify TSC22D4 as a novel Akt1-interacting protein. Glucose and insulin stimulation of the starved cells destabilizes the TSC22D4-Akt1 interaction. In vivo, insulin injection or refeeding of fasted mice is sufficient to weaken the hepatic TSC22D4-Akt1 interaction. Energy deprivation and oxidative stress, on the other hand, promote the TSC22D4-Akt1 interaction. We identified that the C-terminal half of the TSC22D4 intrinsically disordered region (D2 domain) and its TSC box are required to interact with Akt1. At

[1]Joint Heidelberg-IDC Translational Diabetes Program, Inner Medicine 1, Heidelberg University Hospital, Heidelberg, Germany. [2]Institute for Diabetes and Cancer (IDC), Helmholtz Diabetes Center, Helmholtz Center, Munich, Neuherberg, Germany. [3]German Center for Diabetes Research (DZD), Neuherberg, Germany. [4]Research Unit Analytical Pathology, German Research Center for Environmental Health, Institute of Pathology, Helmholtz Zentrum München, Ingolstädter Landstraße 1, 85764 Neuherberg, Germany. [5]Center for Model System and Comparative Pathology (CMCP), Institute of Pathology, University Hospital Heidelberg, 69120 Heidelberg, Germany.
*Corresponding author. Email: bilgen.ekimuestuenel@med.uni-heidelberg.de

the molecular level, TSC22D4-Akt1 interaction promotes insulin sensitivity by reducing basal Akt phosphorylation during starvation. In mice, hepatic TSC22D4-Akt1 interaction improves glucose handling and insulin sensitivity without any changes in body weight.

Overall, on the basis of our findings, we propose a model in which TSC22D4 acts as a signaling molecule that senses the environmental cues to interact with and regulate Akt1 function and glucose metabolism. Our findings shed light on our understanding of molecular mechanisms that underlie the development of insulin resistance and type 2 diabetes, which is key to discovery of novel therapies to treat these modern-day epidemics.

RESULTS

TSC22D4 interacts with Akt1

In our previous studies, we showed that acute TSC22D4 knockdown promoted insulin-induced Akt phosphorylation both in cultured primary hepatocytes and in mouse livers (*7*). To understand the molecular mechanisms of TSC22D4 action on insulin signaling pathway, we examined the functional domains of TSC22D4 protein in detail. TSC22D4 does not contain any domains with a known function other than its TSC box that contains a leucine zipper motif (Fig. 1A). TSC box is common to all TSC22 family members and plays a role in homodimerization or heterodimerization of TSC22 family members with each other (*8*, *16*). By performing Clustal Omega analysis, we identified two other regions region 1 and region 2 (R1 and R2) at the TSC22D4 N terminus, which are highly conserved from fish to mammals (Fig. 1A and fig. S1) (*17*). The primary sequence flanked by R2 and TSC box (105 to 308 amino acids) is also highly conserved between humans and mice yet does not contain any particular three-dimensional structure and falls into the category of intrinsically disordered region (Fig. 1A and fig. S1). Until recently, intrinsically disordered regions were mainly ignored because of the lack of a defined three-dimensional structure, yet these regions contain many different posttranslational modification (PTM) sites (*18*). This diversity and multiplicity of PTMs within intrinsically disordered regions allow proteins to act as critical sensors of the environmental cues, enabling them to act as hubs for cross-talking between signaling pathways.

Because TSC22D4 contains a relatively long stretch of an intrinsically disordered region, we asked whether TSC22D4 interacts with Akt to regulate its function. We prepared whole liver lysates from wild-type (WT) mice and immunoprecipitated (IP) endogenous TSC22D4. We showed that endogenous Akt1 was enriched in endogenous TSC22D4 co-immunoprecipitates (co-IPs) compared to immunoglobulin G (IgG) controls, demonstrating that hepatic TSC22D4 and Akt1 interact in vivo in mouse livers (Fig. 1B). Unlike Akt1, Akt2 failed to enrich as efficiently in the TSC22D4 co-IPs over the IgG controls, indicating that TSC22D4 interacts more specifically with Akt1 rather than Akt2 (Fig. 1B).

Previously, we described a role for hepatic TSC22D4 in regulating glucose metabolism (*7*). To address whether the TSC22D4-Akt1 interaction is also regulated in response to metabolic signals, we performed co-IP experiments with the liver lysates of fasted and refed mice. As shown in Fig. 1C, refeeding of fasted mice impaired the TSC22D4-Akt1 interaction, indicating that blood glucose and insulin levels might play a role in controlling TSC22D4-Akt1 interaction.

To study the regulation of TSC22D4-Akt1 interaction more in detail, we transiently transfected hepatoma 1-6 (Hepa 1-6) cells with Flag-TSC22D4 and HA (Hemagglutinin)-Akt1 or HA-Akt2 plasmids and repeated the co-IP experiments. As shown in Fig. 1D, HA-Akt1 co-IPed with Flag-TSC22D4, and glucose stimulation weakened the TSC22D4-Akt1 interaction. Increasing glucose concentration from 20 to 100 mM did not impair the TSC22D4-Akt1 interaction any further, but additional stimulation of cells with 100 nM insulin did (Fig. 1D, compare lanes 5 to 8 with 11 to 14). In the absence of glucose, insulin alone failed to disrupt the TSC22D4-Akt1 interaction (Fig. 1D, compare lanes 9 and 10 with 11 to 14). Unlike the cells, insulin injection to the starved mice did abolish the TSC22D4-Akt1 interaction, indicating that even fasting blood glucose levels are sufficient to prime the insulin-induced dissociation of TSC22D4-Akt1 interaction (Fig. 1E). Similar to our experiments performed with liver lysates (Fig. 1, B, C, and E), again, we did not detect specific enrichment of HA-Akt2 in Flag-TSC22D4 co-IPs (fig. S1B).Overall, these data indicate that TSC22D4 is a novel Akt1-interacting protein, and metabolic signals such as refeeding or glucose and insulin stimulations impair the TSC22D4-Akt1 interaction both in vivo and in cultured cells.

Energy deprivation promotes TSC22D4-Akt1 interaction

Both in mice and in the cells, TSC22D4 interacted with Akt1 most strongly during starvation, and glucose and insulin stimulations impaired the interaction. Because glucose availability promotes adenosine triphosphate (ATP) generation, we also tested whether mitochondrial function regulates the TSC22D4-Akt1 interaction. We performed Flag-TSC22D4 and HA-Akt1 co-IPs upon pharmacological inhibition of mitochondria with complex I and III inhibitors, rotenone and antimycin, respectively. As shown in Fig. 2A, rotenone and antimycin co-treatment (lanes 6 and 7) promoted the TSC22D4-Akt1 interaction and reduced Akt-S473 phosphorylation while increasing AMPK-T172 phosphorylation, confirming the increase in AMP/ATP ratio. Next, we asked whether inhibition of mitochondria promotes TSC22D4-Akt1 interaction via AMPK activity. To this end, we used U2OS-WT and U2OS-AMPKα1/α2 double knockout (DKO) cells to transiently transfect Flag-TSC22D4 and HA-Akt1 plasmids and repeated co-IP experiments in the presence or absence of rotenone/antimycin. As shown in Fig. 2B, lack of AMPK did not affect rotenone/antimycin-induced TSC22D4-Akt interaction. In addition, glucose and insulin stimulation impaired TSC22D4-Akt interaction to a similar degree in the presence or absence of AMPK (Fig. 2C). Overall, these data suggest that glucose stimulation or inhibition of mitochondria regulates TSC22D4-Akt1 interaction independent of AMPK signaling.

Inhibition of mitochondria also contributes to the generation of reactive oxygen species (ROS) and induces oxidative stress. Hence, we asked whether treatment of cells with ROS would also have an effect on TSC22D4-Akt1 interaction and found out that H_2O_2 treatment of Hepa 1-6 cells robustly promoted TSC22D4-Akt1 interaction (Fig. 2, D and E).

H_2O_2 impairs protein phosphatase 2A (PP2A) activity, which is responsible for removing Akt phosphorylations on T308 and S473 (*19*–*22*). In agreement with these earlier studies, we also observed that H_2O_2 treatment promoted Akt phosphorylation (Fig. 2, D and E). Nevertheless, H_2O_2 elevated Akt phosphorylation to a much less extent in the presence of Flag-TSC22D4 (Fig. 2D, compare lanes 3 with 8 and 9, and Fig. 2E, compare lanes 3 and 4 with 9 and 10), which is consistent with our data in Figs. 1 and 2 (A and B): A weak TSC22D4-Akt interaction associates with elevated Akt phosphorylation,

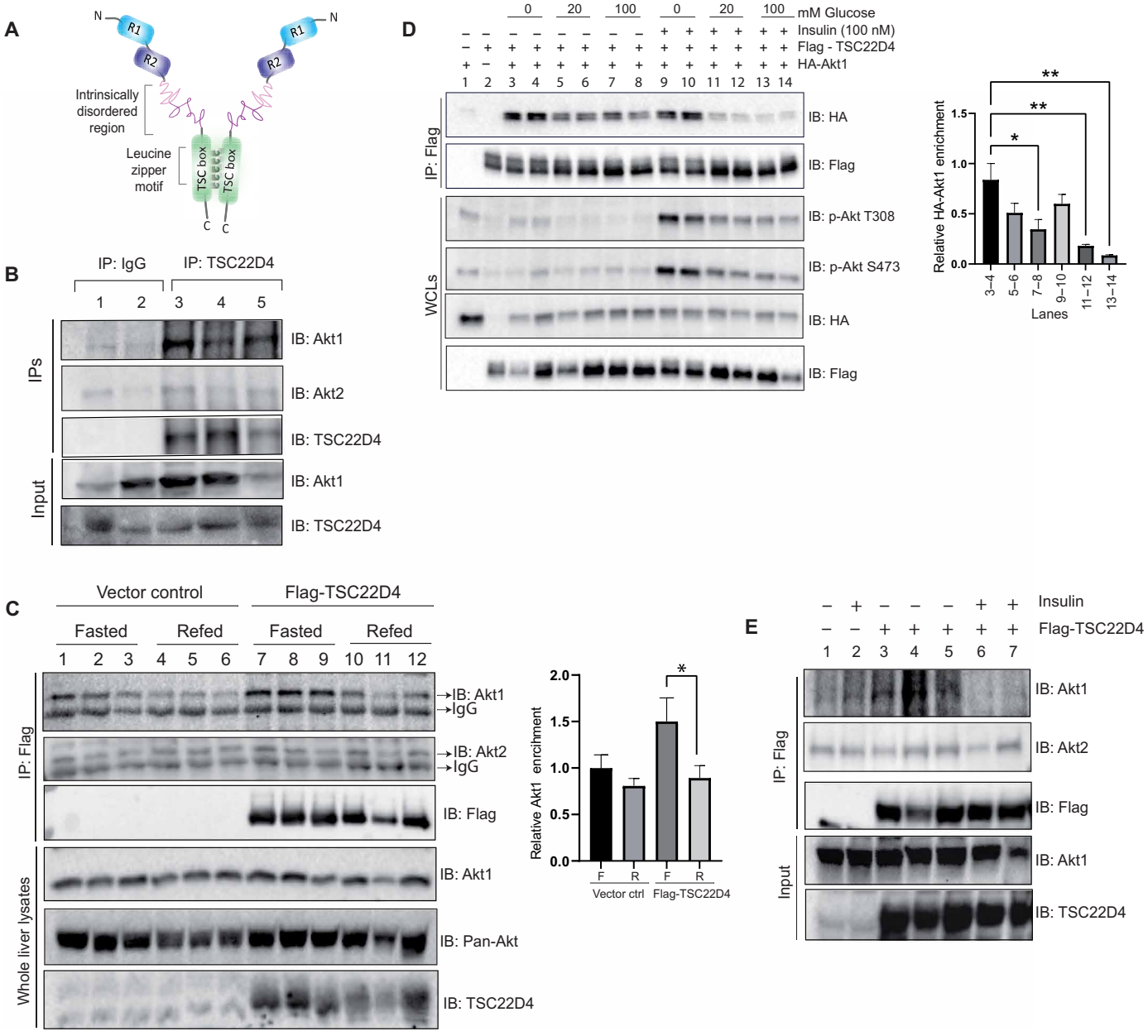

Fig. 1. TSC22D4 interacts with Akt1. (**A**) Illustration of TSC22D4 protein with evolutionarily conserved domains. (**B**) Endogenous TSC22D4 from the wild-type (WT) mouse liver lysates was immunoprecipitated (IP) with TSC22D4 antibody, and the IPs and liver lysates (input) were immunoblotted (IB) with indicated antibodies. Normal rabbit IgG antibody was used as a negative control to TSC22D4 antibody. (**C**) Flag-TSC22D4 was IP from the liver lysates of mice that were injected with adenoviruses (AVs) containing empty vector control or Flag-TSC22D4 cDNA. The mice were starved for 16 hours and refed the next day before euthanasia. The IPs and WCLs were immunoblotted with indicated antibodies. Right: Quantification of Akt1 signal intensity in the IPs normalized to Akt1 signal intensity in the whole liver lysates. F, fasted; R, refed. Statistical analysis: One-way analysis of variance (ANOVA) followed by Sidak's multiple comparison test. *$P < 0.05$. (**D**) Hepa 1-6 cells were transiently transfected with vector control or cotransfected with Flag-TSC22D4 (2.5 μg) and HA-Akt1 (2.5 μg) plasmids. Thirty hours after transfection, cells were serum- and glucose-starved overnight. Cells were pretreated without or with glucose (20 mM) for 30 min and incubated in the absence or presence of insulin (100 nM) for an additional 30 min and then lysed. Flag-TSC22D4 was immunoprecipitated with anti-Flag affinity gel, and the IPs and whole cell lysates (WCLs) were immunoblotted with indicated antibodies. Right: Quantification of HA-Akt1 signal intensity in the IPs normalized to HA-Akt1 signal intensity in the WCLs. Statistical analysis: One-way ANOVA followed by Tukey's multiple comparisons test. *$P < 0.05$ and **$P < 0.001$. (**E**) Flag-TSC22D4 was immunoprecipitated with Flag affinity gel from liver lysates of 6-hour starved and insulin-injected mice (1.3 U/kg for 10 min). IPs and whole liver lysates (input) were immunoblotted with indicated antibodies.

and a strong TSC22D4-Akt1 interaction associates with reduced Akt phosphorylation.

H_2O_2 treatment also induced JNK phosphorylation, indicating the activation of stress signals. Therefore, we also tested whether JNK directly regulates TSC22D4-Akt1 interaction. TSC22D4-Akt1 interaction remained completely intact in JNK1/2 DKO mouse embryonic fibroblasts (MEFs), suggesting that TSC22D4-Akt1 interaction takes place independent of JNK1/2 (fig. S2A). Overall, our findings show that while anabolic signals such as glucose and insulin impair the TSC22D4-Akt1 interaction, catabolic and stress

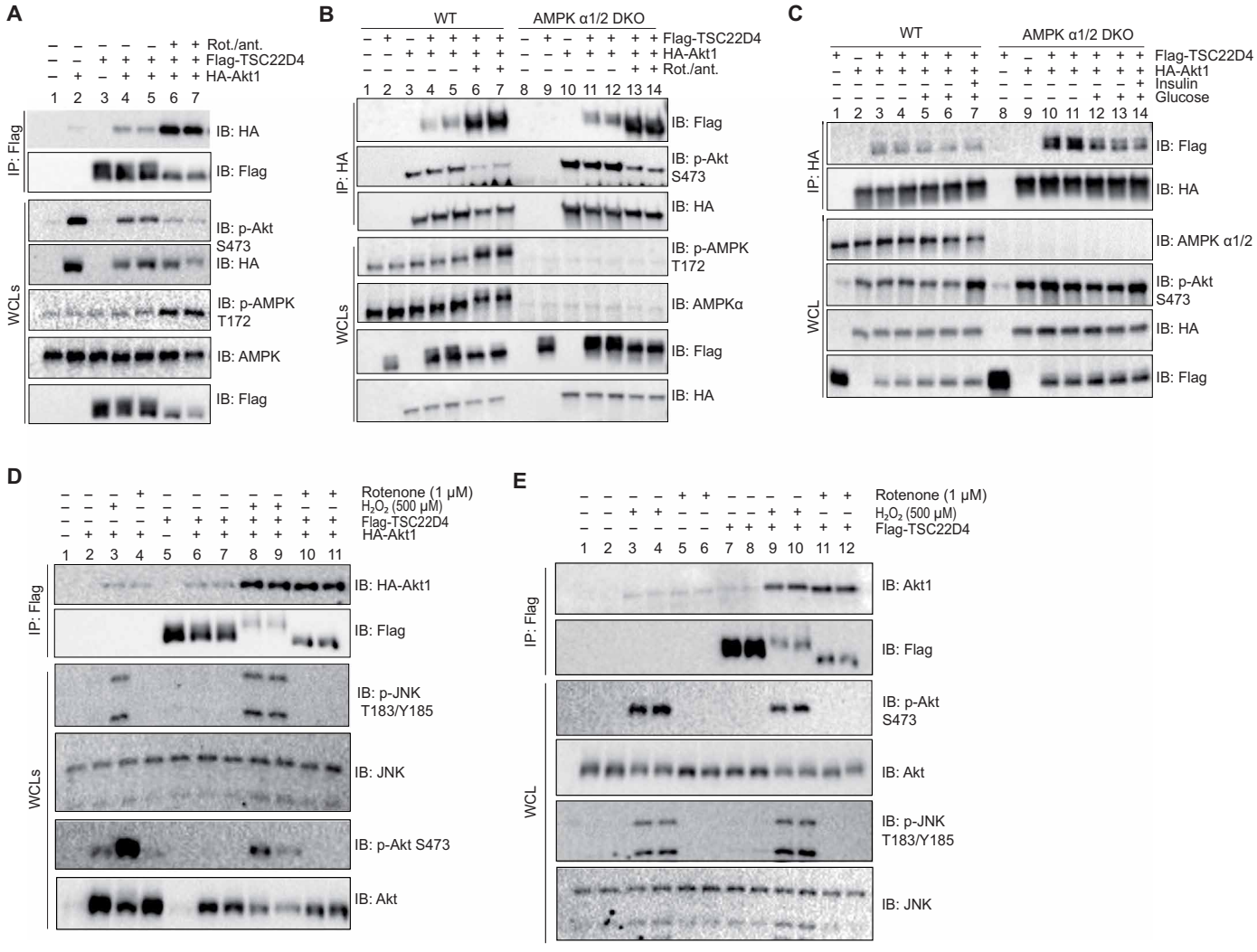

Fig. 2. Energy deprivation and oxidative stress promote TSC22D4-Akt interaction. (**A**) Hepa 1-6 cells were transiently transfected with vector control or cotransfected with Flag-TSC22D4 (2.5 μg) and HA-Akt1 (2.5 μg) plasmids. Thirty hours after transfection, cells were serum- and glucose-starved overnight. Cells were pretreated without or with the rotenone (1 μM)/antimycin (1 μM) mix 1 hour before lysis. Flag-TSC22D4 was immunoprecipitated with anti-Flag affinity gel, and the IPs and WCLs were immunoblotted with the indicated antibodies. (**B**) Similar to (A), except that WT or AMPKα1/2 DKO U2OS cells were used and cells were starved for 4 to 6 hours. IPs were performed with anti-HA antibody. (**C**) WT and AMPKα1/2 DKO U2OS cells were transiently transfected with vector control or cotransfected with Flag-TSC22D4 (2.5 μg) and HA-Akt1 (2.5 μg) plasmids. Forty-eight hours after transfection, cells were serum- and glucose-starved for 4 to 6 hours. Cells were pretreated without or with glucose (20 mM) for 30 min and incubated in the absence or presence of insulin (100 nM) for an additional 30 min and then lysed. HA-Akt1 was immunoprecipitated with anti-HA antibody, and IPs and WCLs were immunoblotted with indicated antibodies. (**D**) Hepa 1-6 cells were transiently transfected with vector control or Flag-TSC22D4 (2.5 μg) and HA-Akt1 (2.5 μg) plasmids. Thirty hours after transfection, cells were serum- and glucose-starved overnight followed by a treatment without or with H_2O_2 (500 μM) or rotenone (1 μM) for an additional 1 hour before lysis. Flag-TSC22D4 was immunoprecipitated with anti-Flag affinity gel, and the IPs and WCLs were immunoblotted with indicated antibodies. (**E**) Same as in (D), except cells were only transfected with vector control or Flag-TSC22D4.

signals promote it, independent of AMPK and JNK signaling pathways, respectively.

Next, we tested whether anabolic or catabolic signals that regulate TSC22D4-Akt1 interaction also control their subcellular localization. Neither with glucose/insulin stimulation nor with rotenone/antimycin treatments, we did not observe any obvious alterations in the subcellular localization of TSC22D4 and Akt1 (fig. S2, B and C). TSC22D4 remained mainly cytoplasmic, whereas Akt1 presented both cytoplasmic and nuclear localization in agreement with previously published studies (*23*–*25*).

TSC22D4-Akt interaction requires TSC22D4 intrinsically disordered region

To map the TSC22D4 domain(s) required for TSC22D4-Akt interaction, we created several TSC22D4 deletion mutants as depicted in Fig. 3A. Because the intrinsically disordered region contains a relatively long stretch of amino acids, we created two segments, domain 1 (D1) and domain 2 (D2) (Fig. 3A). We transiently cotransfected Hepa 1-6 cells with different Flag-TSC22D4 deletion mutants and HA-Akt1. Deletion of R1 (ΔR1) and R2 (ΔR2) individually or together (ΔN) and deletion of the first half of intrinsically disordered

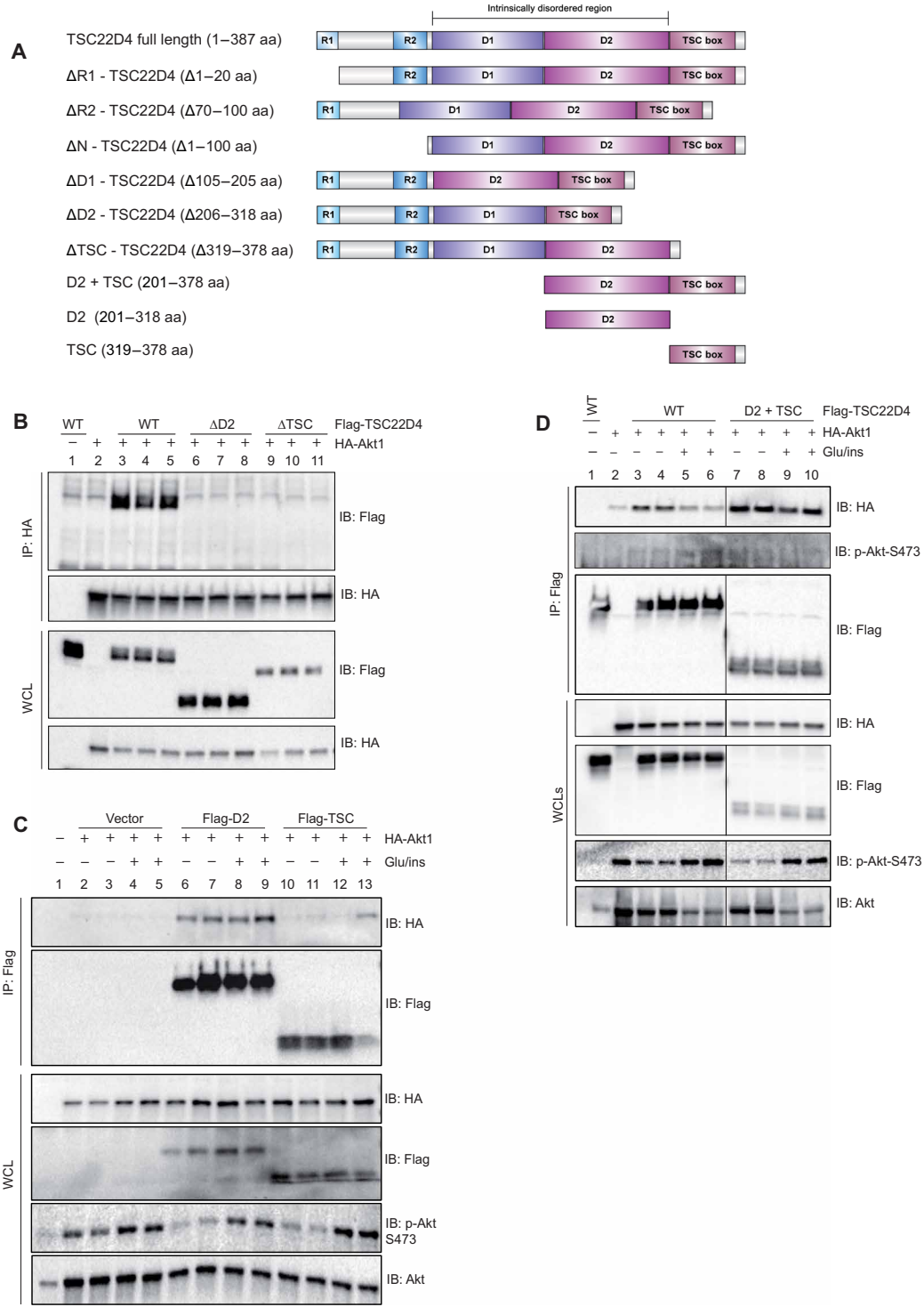

Fig. 3. TSC22D4 D2 domain and TSC box are required for TSC22D4-Akt interaction. (**A**) Illustration of full-length TSC22D4 and deletion mutants we generated. (**B**) Hepa 1-6 cells were transiently cotransfected with Flag-TSC22D4-WT (2.5 μg), Flag-TSC22D4-ΔD2 (2.5 μg), or Flag-TSC22D4-ΔTSC (2.5 μg) deletion mutants and HA-Akt1(2.5 μg). HA-Akt1 was immunoprecipitated with anti-HA antibody, and the IPs and WCLs were immunoblotted with the indicated antibodies. (**C**) Hepa 1-6 cells transiently cotransfected with Flag-tagged empty vector control (4 μg), D2 domain (4 μg), or TSC box (4 μg) truncation mutants and HA-Akt1(1 μg). Thirty hours after transfection, cells were serum- and glucose-starved overnight, and the next day, they were stimulated without or with glucose (20 mM) for 30 min followed by insulin (100 nM) stimulation for another 30 min before lysis. Flag IPs and WCLs were immunoblotted with the indicated antibodies. (**D**) Hepa 1-6 cells transiently cotransfected with Flag-TSC22D4-WT (2.5 μg) or D2 + TSC (2.5 μg) alleles and HA-Akt1 (2.5 μg). Flag-TSC22D4 was immunoprecipitated with anti-Flag affinity gel, and the IPs and WCL were immunoblotted with the indicated antibodies.

region, i.e., ΔD1 did not impair TSC22D4's ability to interact with HA-Akt1, although ΔR2- and ΔN-TSC22D4 mutants were also expressed at very low levels compared to other TSC22D4 alleles (fig. S3A).

Unlike R1, R2, and D1 regions, deletion of D2 (ΔD2) or TSC box (ΔTSC) completely attenuated the TSC22D4-Akt interaction (Fig. 3B). Even when the cells were treated with rotenone and antimycin that boost the TSC22D4-Akt1 interaction, the ΔD2-TSC22D4 mutant failed to interact with Akt completely (fig. S3B). The D2 domain lies within the intrinsically disordered region and potentially carries the necessary features of undergoing versatile PTM events to interact with different partner proteins similar to other intrinsically disordered region proteins. The TSC box, however, plays a key role in homodimerization, which might also be critical for the TSC22D4-Akt1 interaction. The Flag-TSC22D4-ΔTSC mutant failed to dimerize with full-length myc-TSC22D4, confirming its requirement for TSC22D4 homodimerization (fig. S3C). The Flag-ΔD2-TSC22D4, on the other hand, still managed to homodimerize with myc-TSC22D4, albeit to a lesser extent compared to WT Flag-WT-TSC22D4 (fig. S3D). Overall, these data suggest that the TSC domain might have an indirect role in mediating TSC22D4-Akt1 interaction via homodimerization.

Next, we asked whether D2 or TSC domain is sufficient to interact with Akt1. To this end, we generated the truncated mutants of D2 domain and TSC box alone and repeated the co-IP experiments (Fig. 3A). While the D2 domain alone successfully interacted with Akt1, the TSC box alone failed to do so (Fig. 3C). When we combined the D2 and TSC domains to allow homodimerization, we observed that the D2 + TSC mutant interacted with Akt1 more strongly compared to WT-TSC22D4 despite being expressed at lower levels (Fig. 3D), indicating that the N-terminal half of TSC22D4 that is missing in the D2 + TSC mutant might play a negative role in maintaining the TSC22D4-Akt1 interaction. Similar to antimycin/rotenone or H_2O_2 treatments, establishing a stronger TSC22D4-Akt1 interaction with the D2 + TSC mutant again decreased basal Akt phosphorylation in the whole cell lysates (WCLs) (Fig. 3D, compare lanes 3 and 4 with 7 and 8). Although hardly detected in the co-IPs, the phosphorylated Akt (p-Akt) signal intensity within D2 + TSC co-IPs was also lower compared to WT-TSC22D4 co-IPs despite much more enrichment of HA-Akt1.

Overall, these data show that TSC22D4 intrinsically disordered region D2 domain is indispensible and sufficient for TSC22D4-Akt1 interaction. In addition, the TSC22D4 N-terminal region versus the C-terminal region might play opposing effects in regulation of TSC22D4-Akt1 interaction. While the C-terminal end is required to maintain the TSC22D4-Akt1 interaction, the N terminus might actually negatively regulate it. Last, the TSC22D4-Akt1 interaction might control Akt phosphorylation, which we investigated further in primary hepatocytes below.

TSC22D4-Akt1 interaction controls the Akt function

To investigate the role of TSC22D4-Akt1 interaction in Akt signaling further, we isolated primary hepatocytes from TSC22D4$^{hep-/-}$ mice and introduced adenoviral vector control, WT-TSC22D4, ΔD2-TSC22D4, and D2 + TSC alleles. Similar to our observations in Hepa 1-6 cells, the D2 + TSC allele again reduced the basal phosphorylation of Akt and its downstream targets GSK3β and FoxO1 in starved primary hepatocytes (Fig. 4A). Glucose and insulin-induced phosphorylation of Akt and its targets, however, were similar in all groups (Fig. 4B). Notably, because of unclear reasons, the adenoviral ΔD2-TSC22D4 failed to express completely at the protein level; hence, we excluded this allele in the further primary hepatocyte experiments (Fig. 4, A and B, lanes 10 to 12).

To gain further insight into the TSC22D4-mediated regulation of Akt phosphorylation, we asked whether TSC22D4 directly binds to Akt to prevent its mTORC2- and/or PDK1-mediated phosphorylation at S473 or T308, respectively. To this end, we performed in vitro binding assays with Flag-TSC22D4-WT or Flag–D2 + TSC and recombinant His-Akt1. We did not, however, detect any specific enrichment of WT-TSC22D4 and Flag–D2 + TSC or His-Akt1 in His- or Flag- pulldowns, respectively (fig. S4A). In addition, the subcellular localization of Akt1 also did not change upon overexpression of WT-TSC22D4 or D2 + TSC in Hepa 1-6 cells (fig. S4B).

When we induced gluconeogenesis in primary hepatocytes via starvation followed by forskolin/glucagon treatment, TSC22D4-KO cells expressing the D2 + TSC allele secreted lower glucose levels into the medium compared to the vector control or WT-TSC22D4 (Fig. 4C and fig. S4, C and D). Although insulin suppressed glucose production both in TSC22D4$^{flox/flox}$ control and in TSC22D4-KO cells, inhibition of Akt function rescued insulin effect only in control but not in KO cells (Fig. 4C and fig. S4E). These data indicate that hepatocytes with chronic loss of TSC22D4 must have developed some yet-to-be identified mechanisms for insulin-mediated suppression of gluconeogenesis independent of Akt (Fig. 4C). This phenomenon was also observed before by other colleagues, in which insulin was still able to suppress gluconeogenesis in liver-specific Akt and Foxo1 KO mice (*26*). Forskolin treatment also promoted the TSC22D4-Akt1 interaction after treatment for 4.5 hours, particularly with WT-TSC22D4 (Fig. 4D and fig. S4G). Next, we checked the expression of gluconeogenic genes in TSC22D4$^{flox/flox}$ control versus TSC22D4-KO cells in response to forskolin treatment and observed that TSC22D4-KO cells expressing D2 + TSC allele presented higher peroxisome proliferator-activated receptor γ coactivator 1-α (PGC-1α) expression compared to KO cells expressing vector control or WT-TSC22D4 (Fig. 4E and fig. S4F). This elevated PGC-1α expression with D2 + TSC was dependent on Akt function because inhibition of Akt with Akti 1/2 inhibitor promoted induced PGC-1α expression even further, which was also the case in TSC22D-4$^{flox/flox}$ control cells (Fig. 4E).

In addition, in agreement with our previous study, TSC22D4-KO cells expressed PGC-1α, phosphoenolpyruvate carboxykinase 1 (PCK1), and glucose-6-phosphatase (G6P), at much lower levels compared to TSC22D4$^{flox/flox}$ control cells (Fig. 4, E to G) (*7*). PGC-1α acts as a central regulator of energy metabolism and has a dual function in controlling gluconeogenesis. PGC-1α promotes gluconeogenesis by promoting the expression of PCK1 and G6P, which, however, was not the case with the D2 + TSC mutant (Fig. 4, C and E to G). PGC-1α, also, down-regulates gluconeogenesis by modulating the IRS1/IRS2 ratio and Akt function (*27*). Hence, it is possible that elevated PGC-1α expression with the D2 + TSC allele might be acting via the IRS1/IRS2 axis to control Akt function and lower glucose production during starvation.

Overall, these data indicate that promoting a stronger TSC22D4 Akt interaction blunts phosphorylation of Akt and its downstream targets under starvation conditions. In addition, TSC22D4-Akt interaction promotes PGC-1α expression in an Akt-dependent manner and reduces gluconeogenic potential.

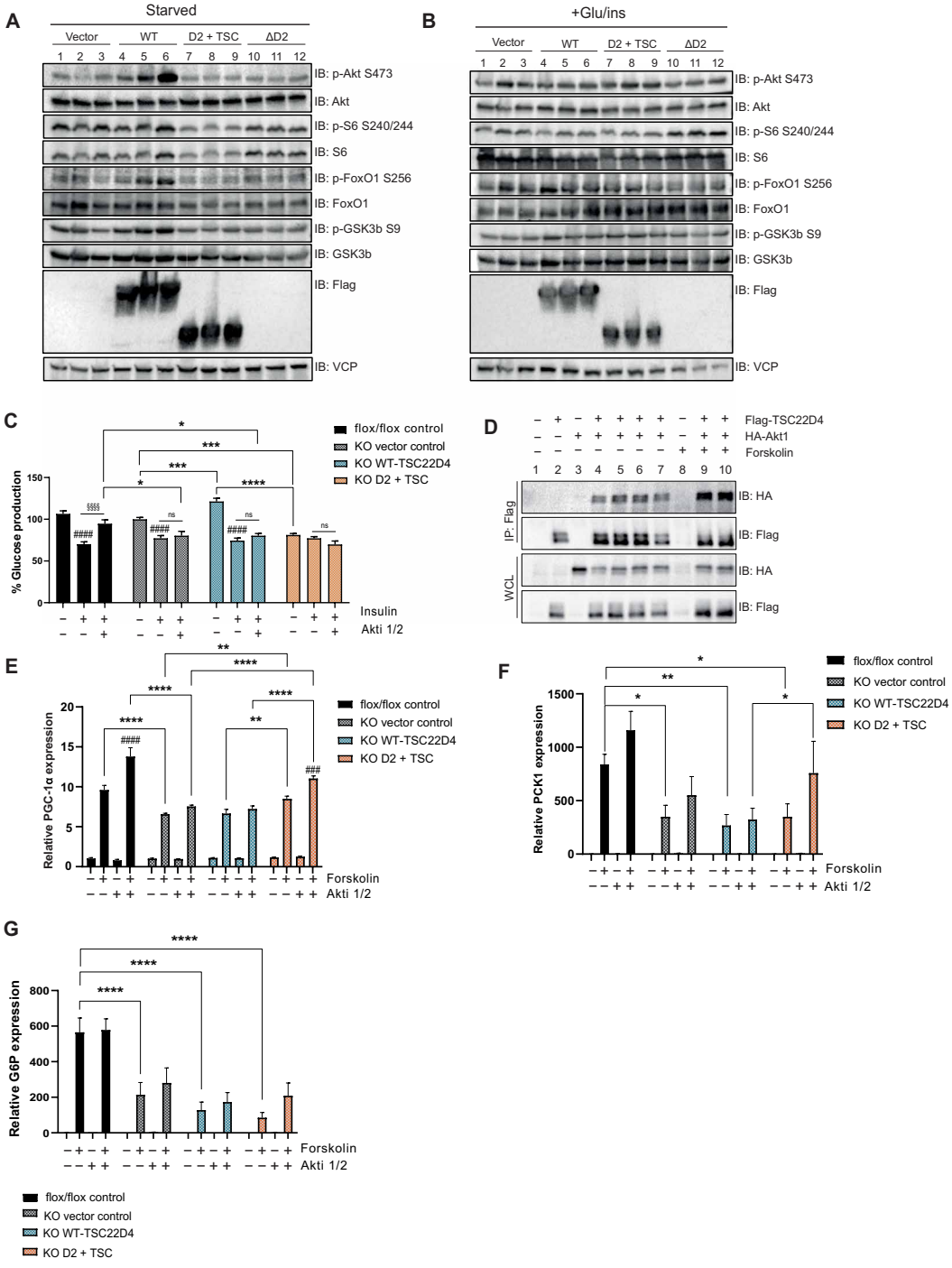

Fig. 4. TSC22D4-Akt1 interaction controls Akt function. (**A**) Primary hepatocytes were transduced with AVs expressing vector control or TSC22D4 alleles. Thirty-six hours after transduction, cells were starved overnight. The next day, cells were lysed and protein extracts were immunoblotted with the indicated antibodies. (**B**) As in (A), except cells were stimulated with glucose (20 mM) for 30 min and insulin (100 nM) for another 30 min before lysis. (**C**) TSC22D4$^{flox/flox}$ control or AV-transduced TSC22D4 KO primary hepatocytes were starved in phenol-free media for 8 hours followed by treatment with gluconeogenic inducers [forskolin (100 μM) and glucagon (100 nM)] in the absence or presence of insulin (100 nM) and/or Akt inhibitor (Akti 1/2) (5 μM) for 12 hours. The medium was collected, and glucose levels were measured via the Amplex Red Kit. Glucose concentration was normalized to the KO cells with vector control. (**D**) Hepa 1-6 cells were cotransfected with Flag-WT-TSC22D4 and HA-Akt1. The cells were starved overnight followed by a dimethyl sulfoxide (DMSO) control or forskolin (100 μM) treatment for 4.5 hours. IPs and WCLs were immunoblotted with indicated antibodies. (**E** to **G**) TSC22D4$^{flox/flox}$ or AV-transduced TSC22D4 KO primary hepatocytes were starved overnight followed by DMSO or forskolin (100 μM) treatment in the presence or absence of Akti 1/2 (5 μM) for 4.5 hours. Cells were collected in TRIzol for RNA isolation, and gene expression was measured by quantitative reverse transcription polymerase chain reaction. Statistical analysis (C and E to G): Two-way ANOVA with Tukey's multiple comparisons test. *$P < 0.05$, **$P < 0.01$, ***/###$P < 0.001$, and ****/####/§§§§$P < 0.0001$. * denotes comparison between different cell populations. # denotes insulin effect within each cell population in (C) and Akti 1/2 effect in forskolin-treated cells in (E) to (G). ns, not significant.

Hepatic TSC22D4-Akt interaction improves glucose metabolism

As shown in Fig. 1, elevated glucose and insulin levels impaired the TSC22D4-Akt1 interaction, and boosting the TSC22D4-Akt1 interaction via D2 + TSC mutant reduced Akt phosphorylation in starved cells (Figs. 3D and 4A). Hence, we addressed whether deregulated TSC22D4-Akt1 interaction has any relevance in insulin-resistant state and checked whether TSC22D4 and Akt1 interacted differentially in control versus high-fat high-sucrose (HF/HS) diet–fed mice (fig. S5, A to D). As shown in Fig. 5A, the endogenous TSC22D4-Akt1 interaction tended to be weaker on average in the livers of mice on an HF/HS diet, which prompted us to investigate the function of TSC22D4-Akt1 interaction in controlling glucose metabolism and insulin sensitivity in vivo.

To this end, we generated adeno-associated viruses (AAVs) by subcloning the cDNAs of TSC22D4 WT (i.e., WT), ΔD2 (i.e., interaction-deficient mutant), and D2 + TSC (i.e., strongly interacting mutant) alleles to AAV serotype 2 vector with hepatocyte-specific Liver-specific promoter 1 (LP1) promoter for hepatocyte-specific targeting of the mouse livers. To avoid potential interference from the endogenous TSC22D4 that would exist in WT mice, we used hepatocyte-specific TSC22D4 KO ($TSC22D4^{hep-/-}$) mice for introduction of TSC22D4 alleles (fig. S5E) (*25*). Similar to our previous findings (*7*), $TSC22D4^{hep-/-}$ mice had improved glucose handling in glucose tolerance test (GTT) and lower fasting blood glucose levels compared to $TSC22D4^{flox/flox}$ control mice when challenged with high-fat diet (HFD) without any changes in body weight (fig. S5, E to H).

We injected $TSC22D4^{hep-/-}$ mice with the AAVs carrying vector control or Flag-TSC22D4 alleles when they were 6 to 8 weeks old (figs. S5I and S6A). We kept the mice on chow diet for the initial 6 weeks and then challenged them with HF/HS diet for another 7 weeks before the experiment ended (Fig. 5B). All mice gained similar amount of weight throughout the experiment, and all Flag-TSC22D4 alleles were expressed at the correct molecular weight (fig. S6, A and B). During the chow diet phase, mice expressing the D2 + TSC allele performed better in GTT and insulin tolerance test (ITT) compared to mice expressing the WT-TSC22D4 (Fig. 5C and fig. S6C). Hepatic expression of the D2 + TSC mutant also led to an improved ITT and GTT profile after 7 weeks of HF/HS diet challenge (Fig. 5D and fig. S6D). When we challenged the mice in a second cohort with HF/HS diet for 12 weeks instead of 7 weeks, the vector control and D2 + TSC–expressing mice again showed an improved GTT and ITT profile compared to mice expressing the WT- or the ΔD2-TSC22D4 mice without any changes in body weight (Fig. 5E and fig. S6, E to G). Because of reduced basal Akt phosphorylation in starved mice, D2 + TSC–expressing livers also showed a much better insulin response at the molecular level compared to mice with WT-TSC22D4 (fig. S6H, compare lanes 3 to 6 versus 11 to 14). InFigs. 1 and 2, we pointed out that energy deprivation promotes the TSC22D4-Akt1 interaction. Hence, by strongly interacting with Akt1, the D2 + TSC allele might actually be mimicking starvation even under conditions of overnutrition, which might alleviate the negative feedback loops and promote insulin sensitivity.

In addition, after 7 weeks of HF/HS diet challenge, overexpression of WT-TSC22D4 elevated the serum insulin levels and exacerbated insulin resistance, which did not take place with the mice expressing the D2 + TSC allele (Fig. 5, F and G). After 12 weeks of HF/HS diet challenge, the WT-TSC22D4–expressing mice no longer had elevated serum insulin and homeostatic model assessment for insulin resistance (HOMA-IR) index compared to the mice expressing the vector control (fig. S6, I and J). Nevertheless, mice expressing D2 + TSC allele still had lower serum insulin levels and an improved HOMA-IR index as opposed to the mice expressing the ΔD2-TSC22D4 (fig. S6, I and J).

Next, we checked the liver lipid levels in mice expressing different TSC22D4 alleles. In agreement with our recent findings (*25*), hepatic overexpression of WT-TSC22D4, but not the D2 + TSC mutant, tended to elevate liver triglycerides upon 7 weeks of HF/HS diet (fig. S7A). When we further evaluated hematoxylin and eosin (H&E)–stained liver sections from the same experiment, we observed that the expression of ΔD2-TSC22D4 significantly elevated the percentage of lipid droplets in the liver sections, which did not take place with the D2 + TSC allele (fig. S7B). Serum alanine transaminase (ALT), aspartate aminotransferase (AST), high-density lipoprotein (HDL), low-density lipoprotein (LDL), and triglycerides (TG) levels remained unaffected in all groups of mice (fig. S7, C to G).

DISCUSSION

Deregulated insulin/Akt signaling pathway plays a key role in pathogenesis of insulin resistance and type 2 diabetes. Here, we found that TSC22D4 is a novel Akt1 binding protein. TSC22D4-Akt1 interaction responds to metabolic signals and regulates Akt function both in cultured cells and in mice. Because TSC22D4 knockdown improves hyperglycemia and insulin resistance in diabetic mice (*7*), we initially hypothesized that the TSC22D4-Akt1 interaction is harmful and impairs metabolic homeostasis. To our surprise, however, we found out that TSC22D4-Akt1 interaction actually plays a positive role and improves glucose metabolism upon HF/HS diet challenge. On the basis of our previous and recent findings, we postulate the following working model (Fig. 6): Under normal conditions, starvation promotes the TSC22D4-Akt1 interaction, which weakens upon high-glucose and high-insulin levels during feeding. During conditions of chronic hyperglycemia and hyperinsulinemia, however, TSC22D4 fails to interact with Akt1 and contributes to insulin resistance and hyperglycemia. Hence, when we knock down TSC22D4 in mouse models for insulin resistance and type 2 diabetes, we see an improved metabolic profile (*7*). When we force the TSC22D4-Akt1 interaction, however, by expressing the D2 + TSC allele, we no longer see its negative effects on glucose metabolism. Overall, establishing a stronger TSC22D4-Akt1 interaction improves glucose handling and alleviates insulin resistance. Similarly, energy deprivation and oxidative stress also elevated the TSC22D4-Akt1 interaction, which might be a mechanism for how physical activity and moderate levels of ROS improve glucose metabolism and insulin sensitivity (*28*, *29*). Perhaps, the strong interaction between D2 + TSC and Akt1 ameliorates metabolic parameters by establishing a pseudo-condition for fasting and physical exercise.

To understand the exact function of TSC22D4-Akt1 interaction, we had to overexpress the TSC22D4 mutants to do functional assays in primary hepatocytes and in mouse liver. The overexpression TSC22D4 protein levels did surpass the endogenous levels (Figs. 4E and 5I). Nevertheless, the levels of ectopically expressed WT-TSC22D4 and D2 + TSC alleles remained always similar in all experimental settings (figs. S4D and S6, A and E), rendering our interpretations valid.

Another intriguing aspect of our study emerged with the use of Akti 1/2 inhibitor in our primary hepatocyte experiments. In all

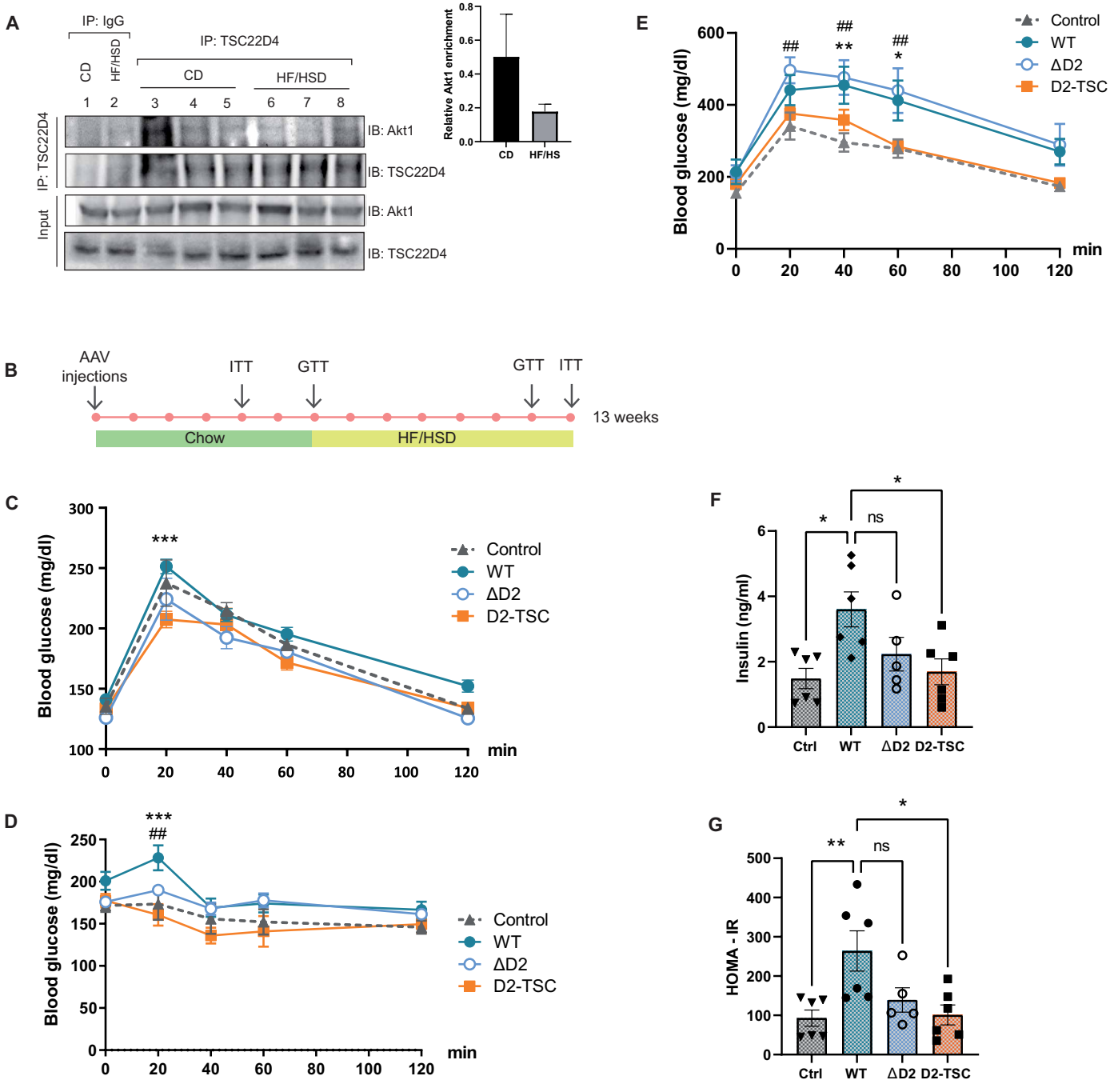

Fig. 5. TSC22D4-Akt1 interaction improves glucose metabolism. (**A**) TSC22D4 was immunoprecipitated from the mouse liver lysates fed with control diet (CD) or HF/HS diet for 26 to 27 weeks. The IPs and the input liver lysates were immunoblotted with indicated antibodies. Right: Quantification of Akt1 enrichment in TSC22D4 co-IPs normalized to Akt1 levels in the input. (**B**) Six- to 8-week-old TSC22D4$^{hep-/-}$ mice were injected with adeno-associated viruses (AAVs) carrying vector control or Flag-TSC22D4 alleles. The mice were kept on chow diet for the initial 6 weeks followed by another 7 weeks of HF/HS diet challenge. Insulin and glucose tolerances tests (ITTs and GTTs) were performed at indicated time points. (**C**) GTT performed with mice at week 6 of AAV injections. (**D**) ITT performed with mice after a HF/HS diet challenge for 7 weeks. ## denotes WT versus vector control; *** denotes WT versus D2 + TSC. (**E**) GTT performed with mice injected with AAVs and challenged with HF/HS diet for 12 weeks. * denotes vector control versus WT; # denotes vector control versus ΔD2. (**F**) Serum insulin levels of mice after 7 weeks of HF/HS diet challenge. (**G**) HOMA-IR index of mice after 7 weeks of HF/HS diet challenge. Statistical analysis (C to E): Two-way ANOVA with repeated measures and Dunnett's multiple comparison test. (F and G): One-way ANOVA followed by Tukey's multiple comparisons test. *$P < 0.05$, **/##$P < 0.01$, and ***$P < 0.001$.

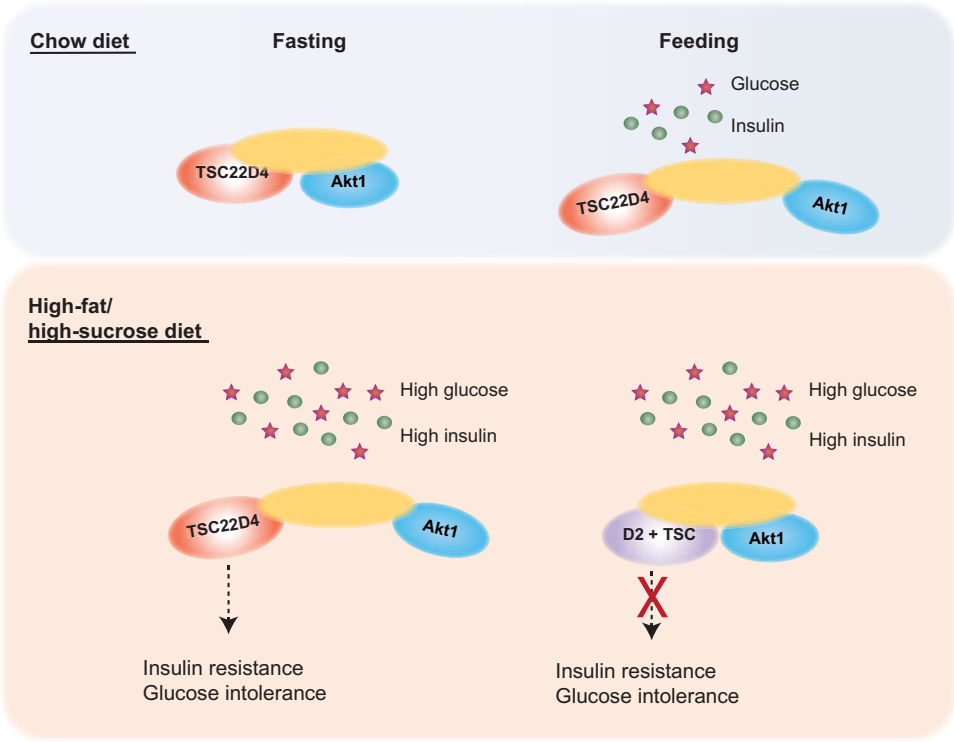

Fig. 6. Working model. TSC22D4 and Akt1 interact indirectly via protein(s) yet to be identified, which is arbitrarily depicted as an orange ellipse. TSC22D4 interacts with Akt most strongly under conditions of energy deprivation. Elevated glucose and insulin levels weaken the TSC22D4-Akt1 interaction. Under conditions of chronic hyperglycemia and hyperinsulinemia, TSC22D4 fails to interact with Akt1 strongly and promotes insulin resistance and impairs glucose handling. Hence, TSC22D4 knockdown in mouse models of type 2 diabetes successfully improves insulin sensitivity and hyperglycemia (*7*). D2 + TSC allele, on the other hand, can still interact with Akt effectively, and unlike WT TSC22D4, it does not exacerbate metabolic parameters.

different cell populations, insulin was able to suppress glucose production, except for D2 + TSC–expressing cells that already secreted much lower glucose. Only in TSC22D4$^{flox/flox}$ control cells but not in KO cells, Akti 1/2 was able to reverse the insulin-mediated suppression of gluconeogenesis (Fig. 4C). These data indicate that TSC22D4-KO hepatocytes must have developed alternative mechanisms in which insulin suppresses gluconeogenesis independent of Akt function. This phenomenon was also observed before by other colleagues, in which insulin still suppressed gluconeogenesis in the absence of Akt and Foxo1 in mice (*26*).

Furthermore, TSC22D4-KO primary hepatocytes expressed gluconeogenic genes PGC1α, G6P, and PCK1 at much lower levels compared to TSC22D4$^{flox/flox}$ control cells, confirming our previous study (*7*). Nevertheless, TSC22D4-KO cells did not generate any less glucose compared to TSC22D4$^{flox/flox}$ control cells in the gluconeogenesis assay (Fig. 4C). This might be because of the presence of extra glucagon in the assay medium, which initiates additional signaling events to promote gluconeogenesis.

Notably, in our former work, we demonstrated that adenoviral overexpression of TSC22D4 in WT mice on a chow diet blunted hepatic Akt phosphorylation under both starved and fed conditions (*7*). In the current study, however, AAV-mediated overexpression of WT-TSC22D4 in HF/HS-challenged TSC22D4$^{hep-/-}$ mice did not necessarily reduce Akt phosphorylation but rather elevated the p-Akt levels during starvation One explanation for this paradoxical observation could be due to overexpressing TSC22D4 in different strains of mice subjected to different diets: WT versus TSC22D4$^{hep-/-}$ mice on a chow versus HF/HS diet, respectively. The hyperglycemic/hyperinsulinemic environment caused by the HF/HS diet might have also prevented a sufficiently strong interaction between WT-TSC22D4 and Akt1 to suppress Akt1 phosphorylation. The method we used to introduce the TSC22D4 alleles could also explain the discrepancy in these mouse experiments; in the previous study, we used adenoviruses (AVs) for liver-specific TSC22D4 overexpression. In the current study, however, we used AAVs for overexpressing TSC22D4 alleles specifically in the hepatocytes within the liver. Similarly, we also observed an increase in p-Akt levels in TSC22D4-KO primary hepatocytes expressing Flag-WT-TSC22D4 (Fig. 4A), which could only survive overnight starvation in the presence of low-glucose/low–fetal bovine serum (FBS) medium. We suspect that the presence of glucose and FBS even at minimal levels prevents a strong WT-TSC22D4-Akt interaction; and does not cause a decrease in p-Akt levels. TSC22D4 might also have dual functions to control Akt phosphorylation, such as the mTOR-Raptor interaction within mTORC1. As in the TSC22D4-Akt interaction, mTOR-Raptor interaction also weakens in response to nutrients (*30*). Although a very strong mTOR-Raptor interaction impairs mTORC1 function, mTOR still requires Raptor to phosphorylate its downstream targets (*30*). Hence, reintroducing TSC22D4 to TSC22D4-KO primary hepatocytes or livers might also promote Akt phosphorylation in a similar manner. Furthermore, the chronic loss of TSC22D4 in the hepatocytes could also have developed some compensatory mechanisms that might

cause additional discrepancies. Nevertheless, in both studies, hepatic overexpression of WT-TSC22D4 impaired glucose metabolism and exacerbated insulin resistance (Fig. 5 and fig. S6) (*7*).

Unlike the changes in insulin resistance and glucose handling, we did not observe any major discrepancies in liver lipid accumulation in our mouse experiments. Our in vivo functional assays depend on the ectopic expression of TSC22D4 alleles in the livers. AAV-mediated gene expression tends to diminish within 12 to 14 weeks of injections, which limits the duration of HF/HS diet regimen to a relatively short time period compared to other HF/HS studies in the field. Hence, the 12 weeks of HF/HS diet regimen might be too short to see a robust difference in liver lipid accumulation.

Akt2 is the other form of Akt ubiquitously expressed in the liver. In our co-IP experiments, we did not observe any specific interaction between TSC22D4 and Akt2. Earlier studies suggest that Akt2 regulates glucose metabolism, while Akt1 regulates cell survival and proliferation (*31*–*33*). These conclusions, however, rely mainly on whole-body KO experiments, which might be misleading in terms of defining organ-specific functions of Akt isoforms. In addition, data from Birnbaum laboratory challenge this concept by showing that deletion of hepatic Akt1 also leads to insulin resistance and hyperglycemia, validating the physiological relevance of our findings (*26*).

One of the open questions remaining in our study is the following: How exactly TSC22D4 impairs Akt phosphorylation? One potential hypothesis would be TSC22D4 directly binds to Akt to prevent its access by mTORC2 or PDK1. However, we could not detect any direct TSC22D4-Akt1 interaction in our in vitro assays. (fig. S4A). TSC22D4 contains a long stretch of intrinsically disordered region with multiple PTM sites (*9*), which might enable it also to interact with other Akt regulators such as PDK1 and mTORC2 or PP2A to control Akt phosphorylation.

Overall, our study contributes to a better understanding of molecular mechanisms that govern the pathogenesis of insulin resistance, which is key to the development of novel therapies to treat type 2 diabetes and its long-term complications. It might be interesting to unravel, in the future, whether TSC22D4-Akt1 interaction also contributes to pathogenesis of other diseases such as cancer in which deregulated Akt1 functions plays a central role.

MATERIALS AND METHODS

Animal experiments

Male albumin-cre mice crossed to the TSC22D4 floxed/floxed ($TSC22D4^{flox/flox}$) line (C57Bl/6N background) (*25*) were housed at room temperature (RT) with 12-hour light–12-hour dark cycle on control diet (Research Diets, New Brunswick, NJ, USA; D12450B), 60% HFD (Research Diets, D12492i) with sucrose-containing drinking water (42 g/liter), or chow diet (10% energy from fat; Research Diets, D12450Ji) for weeks indicated for each study. Mice had ad libitum access to food and water and were weighed regularly and inspected daily for general health. All experiments were performed in accordance with the European Union directives and the German Animal Welfare Act (Tierschutzgesetz) and were approved by local authorities (Regierungspräsidium Karlsruhe, license #G117/18 or #G116/18).

For AV injections, 2×10^9 plaque-forming units per recombinant virus were administered via tail vein injection. In each experiment, 4 to 12 animals received identical treatments and were analyzed under fasted, random fed, or fed conditions as indicated. Organs including the liver, epididymal and inguinal fat pads, and gastrocnemius muscles were collected after specific time periods, weighed, snap-frozen, and used for further analysis.

AAVs were injected via tail vein at a dose of at 1×10^{10} vector genome per mouse. Intraperitoneal ITTs and GTTs were performed at different time points. After mice were starved for 6 hours in the morning, either glucose was intraperitoneally injected at a dose of 1 g/kg (for GTTs) or insulin solution was injected at a dose of 0.75 U/kg for chow diet–fed mice or at 1.3 U/kg for HF/HS diet–fed mice (for ITTs). Before euthanizing after 12 to 13 weeks of AAV injection, mice were starved for 6 hours and followed by intraperitoneal injection with insulin (1 or 1.3 U/kg mouse body weight) or control saline solution for 10 min. Organs including the liver, epididymal fat pads, kidney, pancreas, and gastrocnemius muscles were collected after specific time periods, weighed, snap-frozen, and used for further analysis. In each animal experiment, mice were randomly assigned to each group.

During animal group allocation, animals in each group had similar mean and median body weight and fasting blood glucose levels. Animal experiments involved two cohorts of studies with each experimental group containing five to six biological replicates.

Recombinant viruses

AVs expressing the Flag-TSC22D4 alleles (WT, ΔD2, and D2 + TSC) under the control of the cytomegalovirus promoter were cloned using the BLOCK-iT adenoviral expression system (Invitrogen). Viruses were purified by the cesium chloride method and dialyzed against phosphate-buffered saline buffer (PBS) containing 10% glycerol before animal injection, as described (*34*).

For generating AAVs with cDNAs of TSC22D4, alleles (WT, ΔD2, and D2 + TSC) were amplified with the following primer pairs followed by Nhe 1 and Xba 1 digestion and subcloning into pdsAAV-LP1 plasmid (*35*): TSC22D4-AAV with Nhe I: forward, gatgctagcgtgtgctggaattctg; TSC22D4-AAV with Xba I: reverse, gcatctagactcgagtcagatggaggg. The successful clones sequenced for confirmation with the following primers: pdsAAV-TSC: forward, ctgataggcacctattggtc; reverse, ccacaactagaatgcagtg. Once the sequence is confirmed, the plasmids were purified using QIAGEN Megaprep kit (#12381) according to the manufacturer's instructions and sent to Vigene Biosciences (Maryland, USA) for AAV generation, purification, and titration.

Primary hepatocyte isolation and treatment

Primary hepatocytes were isolated as previously described (*36*, *37*). To investigate insulin signaling pathway, primary hepatocytes were seeded to collagen-coated six-well plates (1×10^6 cells per well) in William's E medium (Pan Biotec, #P04-29510) supplemented with 2 mM L-glutamine, 100 nM dexamethasone, 10% FBS (Life Technologies, #10270-106), and 1% penicillin-streptomycin (PenStrep; Life Technologies, #15140122). After 4 hours, the cells were washed two times with PBS to get rid of the cells that do not attach to the surface. For AV transduction, the next day, primary hepatocytes of $TSC22D4^{hep-/-}$ mice were transduced with AVs expressing empty vector control, WT-TSC22D4, ΔD2-TSC22D4, or D2 + TSC constructs (at a multiplicity of infection of 10). After 36 hours of incubation, the cells were starved in Dulbecco's modified Eagle's medium (DMEM) (Life Technologies, #A1443001) supplemented with 5 mM D-glucose, 2 mM L-glutamine, 0.5% FBS, and 1% PenStrep overnight. The next day, the cells were either remained starved or stimulated

with glucose (20 mM) for 30 min and insulin (100 nM) for another 30 min before cell lysis. The cells were collected in 180 μl of 1.5× sample buffer, boiled at 95°C for 5 min, and kept at −20°C until use for Western blotting.

Glucose secretion assay

Primary hepatocytes were seeded in 24-well plates (200,000 cells per well) in collagen monolayer in Williams E medium (Pan Biotec, #P04-29510) containing 100 nM dexamethasone, 10% FBS, and 1% PenStrep. The next day, the cells were transduced with AVs expressing TSC22D4 alleles at a multiplicity of infection of 10 as described above. After 36 hours posttransfection, the medium was changed to phenol-free DMEM supplemented with 0.5% FBS, 5 mM glucose, and 4 mM glutamine for starvation for 8 hours. Then, the cells were washed two times with PBS and added 200 μl of DMEM supplemented with 4 mM glutamine, 2 mM pyruvate, 20 mM lactate (basal medium) and 100 nM glucagon, 100 nM dexamethasone, and 100 μM forskolin for stimulation and another group with 100 nM glucagon, 100 nM dexamethasone, 100 μM forskolin, and 100 nM insulin in the absence or presence of 5 μM Akti 1/2 inhibitor (Tocris, #5773). After 12 hours of incubation, the medium was collected and centrifuged at 6000 rpm for 2 min at RT. The supernatant was collected and stored at −20°C until glucose determination assay (Amplex Red glucose assay kit; Life Technologies, #A22189). The cells that remained in the 24-well plates were added TRIzol to be analyzed further in mRNA level. Glucose secretion assay was performed with at least three biological replicates and four to six technical replicates in each experiment.

Serum measurements

Serum triglyceride, HDL, LDL, ALT, and AST levels were measured on the AU480 chemistry analyzer (Beckman Coulter) using commercially available kits (Beckman Coulter) (*38*). Insulin levels were determined using a mouse insulin enzyme-linked immunosorbent assay (ALPCO, #80-INSMS-E01, E10). HOMA-IR index was calculated on the basis of this formula

$$\text{HOMA-IR}\ (\text{mM}^{-1} \times \mu\text{U ml}^{-1}) = \text{fasting glucose}\ (\text{mM}^{-1}) \times \text{fasting insulin}\ (\mu\text{U ml}^{-1})/22.5$$

Tissue lipid extraction

Hepatic lipids were extracted using frozen liver samples as described before (*39*). Triglyceride levels were determined using commercial kits (Human, #10724). Before lipid extraction, the weight of aliquoted liver for lipid extraction was measured, and the end values were normalized to initial aliquoted liver weight (milligrams).

Cell lines and cell culture

U2 osteosarcoma [U2OS, American Type Culture Collection (ATCC), HTB-96], Hepa 1-6 (ATCC, CRL-1830), human embryonic kidney 293A (HEK293A), and MEF cell lines were used. U2OS (WT and AMPKα1/α2 DKO) cells were a gift from R. Shaw (Salk Institute for Biological Studies, San Diego, CA, USA). WT and JNK1/2 DKO MEFs were a gift from P. Angel (German Cancer Research Center, DKFZ, Heidelberg, Germany). All cell lines were maintained in DMEM (Gibco, #11995) supplemented with 10% heat-inactivated FBS and PenStrep (50 U/ml; Life Technologies, #15140122). HEK293A cells (Thermo Fisher Scientific, #R70507) were used to generate AVs. All the cell lines were maintained at humidified 37°C incubator containing 5% CO_2.

Plasmid DNA transfection

pcDNA3-HA-Akt1 plasmid was a gift from D. Fingar (University of Michigan, Ann Arbor, USA). Expression vectors of WT-TSC22D4 and deletion mutants of TSC22D4 were created using pcDNA3 plasmid backbone. For deletion mutants, site-directed mutagenesis experiments were performed with standard polymerase chain reaction–based methods (New England Biolabs, #E0554S) using corresponding primer sets in Table 1 below.

Plasmids expressing TSC22D4 alleles and Akt1 were transiently cotransfected to Hepa 1-6 cells using Lipofectamine 2000 (Invitrogen, #11668019) according to the manufacturer's instructions. For starvation experiments, 30 hours after transfection, the cells were starved in no glucose-containing RPMI in the absence of FBS (Gibco, #11879020) overnight, and the next day, cells were prestimulated with glucose (20 mM) for 30 min and with insulin (100 nM) for an additional 30 min followed by cell lysis. For experiments that did not involve starvation, cells were lysed 48 hours after transfection. For U2OS cells, the same transfection protocol was followed except that the cells were starved for 6 hours.

Cell or tissue lysis and co-immunoprecipitation

For co-IP experiments, cells and frozen liver tissues were lysed in ice-cold lysis 3-[(3-cholamidopropyl)dimethylammonio]-1-propanesulfonate (CHAPS) buffer containing 10 mM KPO_4 (pH 7.2), 1 mM EDTA, 5 mM EGTA, 10 mM $MgCl_2$, 50 mM β-glycerophosphate, and 0.3%

Table 1. Custom-designed primer pairs to generate TSC22D4 deletion and truncation mutants.

Deletion mutants	Forward primer	Reverse primer
TSC22D4-ΔR1	GAGGGCCCAGGAAGCCCAG	GGCCGCTGGCTTGTCATCGTC
TSC22D4-ΔR2	GAGCCTCCAAGCTTCGGT	GGCAGGGGCTCCAGGT
TSC22D4-ΔN	GAGCCTCCAAGCTTCGGT	GGCCGCTGGCTTGTCATCGTC
TSC22D4-ΔD1	ACCCTGCCCTCTCTGAGG	GCTTGGAGGCTCCAGATC
TSC22D4-ΔD2	GACTTGGTGAAGTCCCAC	CTGAGCACTATCTCCAGT
Truncation mutants		
D2 + TSC	GGAGATAGTGCTCAGACCCTG	GGCCGCTGGCTTGTCATCGTC
D2 domain	CCCTCTGCACCCAATGGGC	CATGGCTTGTTCAATCTTGTTGT
TSC box	GACTTGGTGAAGTCCCACCTCATG	GGCCGCTGGCTTGTCATCGTC

CHAPS supplemented with cOmplete protease inhibitor cocktail (Roche, #11836145001) and PhosSTOP EASYpack phosphatase inhibitor (Roche, #4906837001). Lysed cells or liver tissue were centrifuged at 12,000 rpm for 5 min at 4°C, and supernatants were collected. Protein concentrations were measured with Bradford (Bio-Rad, #5000006) or Bicinchoninic acid assay (BCA) assay (Pierce, #23227). For immunoprecipitation of transfected cell lysates, anti-Flag affinity gel (Sigma-Aldrich, #A2220) or HA-conjugated agarose beads (Sigma-Aldrich, #A2095) were used. Before use, the beads were washed with lysis buffer via centrifugation at 4000 rpm for 2 min. For immunoprecipitation, cell lysates were incubated with the beads for 2 hours at 4°C on a rotator. The beads were washed three times with ice-cold co-IP lysis buffer with centrifugation steps in between. Laemmli buffer (2×) was added to the samples that then were boiled at 95°C for 5 min.

Liver lysates of mice were prepared to analyze the endogenous interaction of TSC22D4-Akt1. Rabbit IgG control (1 mg/ml) [Cell Signaling Technology (CST), #2729S] or TSC22D4 antibody (1 mg/ml; Pineda, home-made antibody) was incubated with liver lysates at 4°C overnight on a rotating rack. The next day, protein A/G beads (Santa Cruz Biotechnology, #sc-2003) were conjugated to protein-antibody complex with 2 hours of incubation at 4°C on a rotating rack. The lysates were washed three times with lysis buffer, added 70 μl of 2× Laemmli sample buffer, and then boiled at 95°C for 5 min. All co-immunoprecipitation experiments were performed with at least three different biological replicates and at least three to four technical replicates for each cell culture experiment.

In vitro binding assays

Hepa 1-6 cells cultured on 60-mm dishes were transiently transfected with vector control, Flag-TSC22D4-WT, or Flag-D2 + TSC alleles (5 μg per dish) at ~70% confluency. Two days after transfection, cells were lysed with the lysis buffer described for co-IP experiments above. The cell lysates were incubated with commercially available recombinant His-Akt1 (1 μg per reaction) (Millipore, #14-276) for 2 hours rotating at 4°C followed by one more hour of incubation in the presence of Ni-NTA His-Tag agarose beads (QIAGEN, #R90115) or Flag affinity gel (Sigma-Aldrich, #A2220). The pull-down assays were washed three times afterward with ice-cold lysis buffer, and the beads were resuspended in 1× sample buffer and boiled at 95°C for 5 min. In vitro binding assays were performed at least three times, with technical duplicates in each experiment.

Western blot analysis

Protein extracts and immunoprecipitates were run on 10% (Bio-Rad, #4561036) or any kilodalton (Bio-Rad, #4569036) of precast protein gels in SDS buffer followed by electrophoretic transfer of proteins to the nitrocellulose membrane (Bio-Rad, #2895). After blocking in 5% nonfat dried milk diluted in tris-buffered saline and 1% Tween 20 (TBS-T) for 1 hour at RT, the membranes were incubated with primary antibodies specific for TSC22D4 (homemade by PINEDA Antibody Service), Flag-HRP (#A8592, Sigma-Aldrich), HA (#2999, CST), Myc (#2040, CST), p-Akt (S473) (#4060, CST), p-Akt (T308) (#13038, CST), Akt (#9272,CST), p-GSK3 β (S9) (#05-643, Upstate), GSK3 beta (#05-412, Upstate), p-Foxo1 (S256) (#9461, CST), Foxo1 (#2880, CST), p-p70S6K1 (#9234, CST), p70S6K1 (#9209, CST), p-S6 (#2271, 2215), S6 (#2217, CST), p-AMPKα T172 (#2531, CST), AMPKα (#2532, CST), and valosin containing protein (VCP) (ab11433, Abcam). Primary antibodies were incubated in 3% bovine serum albumin overnight at 4°C on a rocker. After washing three times with TBS-T each for 10 min, membranes were incubated with horseradish peroxidase (HRP)–conjugated secondary antibodies targeting rabbit or mouse IgG for 1 hour at RT. To avoid background noise in endogenous co-IP experiments, HRP-conjugated veriblot (Abcam, #131366) or rabbit light chain (CST, #93702) was used as secondary antibody. Immunoblots were developed using ECL Western blotting substrate (Sigma-Aldrich, #GERPN2209 or Amersham, #GERPN2236). ChemiDoc Imaging System (Bio-Rad) was used to detect and analyze chemiluminescence signals. Image Lab software from Bio-Rad was used to quantify the Western blot signal intensities.

Immunofluorescence

Flag-TSC22D4 transfected Hepa 1-6 cells were seeded (5000 cells per well) into four-well chamber slides (Thermo Fisher Scientific, #154526). After overnight starvation, the cells were stimulated either with glucose (20 mM) for 30 min and with insulin (100 nM) for another 30 min or with rotenone and antimycin (1 mM) for 1 hour. Then, the cells were fixed in 4% Histofix (Roti, #P087) for 15 min at RT in a humidified chamber. After washing two times with PBS for 5 min, they were permeabilized with 0.25% Triton X-100 (Sigma-Aldrich, #T9284) in PBS for 5 min at RT. After washing two times with PBS, the cells were incubated in blocking solution (10% horse serum in PBS) for 30 min at 37°C. Then, the cells were incubated with primary antibody [anti-Flag (1:1000; Sigma-Aldrich, #F1804)] in 5% horse serum in PBS for 2 hours at 37°C. Following the PBS wash, the cells were incubated in secondary antibody [Alexa Fluor 488 goat anti-mouse (1:5000; Invitrogen, #A11029)] in 5% horse serum in PBS for 1 hour at 37°C. After the final PBS wash, three times each for 5 min, the chambers were mounted with mounting media containing 4A,6-diamidino-2-phenylindole (Invitrogen, #P36935). The cells were analyzed by a Zeiss fluorescent microscope with ×40 magnification and imaged with Zen software. Negative controls for the immunostaining experiments were performed by omitting primary antibodies.

Endogenous Akt1 was stained in starved, glucose/insulin-, and rotenone/antimycin-stimulated cells. Five thousand cells per well were seeded into four-well chamber slides. As described above, the cells were incubated in blocking solution, followed by incubation with primary antibody (anti-Akt1, CST, #2938; 1:1000) and secondary antibody (Alexa Fluor 568 goat anti-rabbit; 1:2000). Cells then were mounted and imaged as described above. Immunofluorescence experiments were performed with two to three different biological replicates, each experiment containing technical duplicates or triplicates.

H&E staining

After overnight fixation in 10% buffered formalin, representative specimens of the liver were routinely dehydrated, embedded in paraffin, and cut into 4-μm-thick sections. All tissue sections were stained with H&E according to a standard protocol.

Lipid droplet analysis

Quantification of lipid amount was morphometrically determined on H&E-stained liver sections following a previously published procedure (*40*, *41*). The H&E-stained tissue sections were scanned with an AxioScan.Z1 digital slide scanner (Zeiss, Jena, Germany) equipped with a ×20 magnification objective and evaluated by digital

image analysis (Definiens Developer XD 2, Definiens AG, Germany). The calculated parameter was the percentage of surface areas considered as lipid droplets divided by the surface area of the entire analyzed liver tissue for each sample.

Software and data analysis

Adobe Illustrator and IBS (Illustrator for Biological Sequences) programs were used to create figures and cartoons of deletion mutants.

Image editing

For some figures, irrelevant lanes were removed from Western blot images. These modifications were indicated with a thin black line on Western blot figures.

SUPPLEMENTARY MATERIALS

Supplementary material for this article is available at https://science.org/doi/10.1126/sciadv.abo5555

View/request a protocol for this paper from *Bio-protocol*.

REFERENCES AND NOTES

1. B. D. Manning, A. Toker, AKT/PKB signaling: Navigating the network. *Cell* **169**, 381–405 (2017).
2. B. D. Manning, L. C. Cantley, AKT/PKB signaling: Navigating downstream. *Cell* **129**, 1261–1274 (2007).
3. K. Du, P. N. Tsichlis, Regulation of the Akt kinase by interacting proteins. *Oncogene* **24**, 7401–7409 (2005).
4. T. Jahn, P. Seipel, S. Urschel, C. Peschel, J. Duyster, Role for the adaptor protein Grb10 in the activation of Akt. *Mol. Cell. Biol.* **22**, 979–991 (2002).
5. K. Du, S. Herzig, R. N. Kulkarni, M. Montminy, TRB3: A tribbles homolog that inhibits Akt/PKB activation by insulin in liver. *Science* **300**, 1574–1577 (2003).
6. S. Demir, P. P. Nawroth, S. Herzig, B. Ekim Üstünel, Emerging targets in type 2 diabetes and biabetic complications. *Adv. Sci.* **8**, e2100275 (2021).
7. B. Ekim Üstünel, K. Friedrich, A. Maida, X. Wang, A. Krones-Herzig, O. Seibert, A. Sommerfeld, A. Jones, T. P. Sijmonsma, C. Sticht, N. Gretz, T. Fleming, P. P. Nawroth, W. Stremmel, A. J. Rose, M. Berriel-Diaz, M. Blüher, S. Herzig, Control of diabetic hyperglycaemia and insulin resistance through TSC22D4. *Nat. Commun.* **7**, 13267 (2016).
8. H. A. Kester, C. Blanchetot, J. den Hertog, P. T. van der Saag, B. van der Burg, Transforming growth factor-beta-stimulated clone-22 is a member of a family of leucine zipper proteins that can homo- and heterodimerize and has transcriptional repressor activity. *J. Biol. Chem.* **274**, 27439–27447 (1999).
9. S. Canterini, V. Carletti, S. Nusca, F. Mangia, M. T. Fiorenza, Multiple TSC22D4 iso–/phospho-glycoforms display idiosyncratic subcellular localizations and interacting protein partners. *FEBS J.* **280**, 1320–1329 (2013).
10. S. Canterini, A. Bosco, V. Carletti, A. Fuso, A. Curci, F. Mangia, M. T. Fiorenza, Subcellular TSC22D4 localization in cerebellum granule neurons of the mouse depends on development and differentiation. *Cerebellum* **11**, 28–40 (2012).
11. J. Dragotto, S. Canterini, P. Del Porto, A. Bevilacqua, M. T. Fiorenza, The interplay between TGF-β-stimulated TSC22 domain family proteins regulates cell-cycle dynamics in medulloblastoma cells. *J. Cell. Physiol.* **234**, 18349–18360 (2019).
12. S. Canterini, A. Bosco, V. De Matteis, F. Mangia, M. T. Fiorenza, THG-1pit moves to nucleus at the onset of cerebellar granule neurons apoptosis. *Mol. Cell. Neurosci.* **40**, 249–257 (2009).
13. D. F. Fiol, S. K. Mak, D. Kultz, Specific TSC22 domain transcripts are hypertonically induced and alternatively spliced to protect mouse kidney cells during osmotic stress. *FEBS J.* **274**, 109–124 (2007).
14. X. Zhang, N. Koga, H. Suzuki, M. Kato, Promotion of cellular senescence by THG-1/TSC22D4 knockout through activation of JUNB. *Biochem. Biophys. Res. Commun.* **522**, 897–902 (2020).
15. A. Jones, K. Friedrich, M. Rohm, M. Schäfer, C. Algire, P. Kulozik, O. Seibert, K. Müller-Decker, T. Sijmonsma, D. Strzoda, C. Sticht, N. Gretz, G. M. Dallinga-Thie, B. Leuchs, M. Kögl, W. Stremmel, M. B. Diaz, S. Herzig, TSC22D4 is a molecular output of hepatic wasting metabolism. *EMBO Mol. Med.* **5**, 294–308 (2013).
16. T. Yasukawa, A. Tsutsui, C. Tomomori-Sato, S. Sato, A. Saraf, M. P. Washburn, L. Florens, T. Terada, K. Shimizu, R. C. Conaway, J. W. Conaway, T. Aso, NRBP1-containing CRL2/CRL4A regulates amyloid β production by targeting BRI2 and BRI3 for degradation. *Cell Rep.* **30**, 3478–3491.e6 (2020).
17. H. McWilliam, W. Li, M. Uludag, S. Squizzato, Y. M. Park, N. Buso, A. P. Cowley, R. Lopez, Analysis tool web services from the EMBL-EBI. *Nucleic Acids Res.* **41**, W597–W600 (2013).
18. P. E. Wright, H. J. Dyson, Intrinsically disordered proteins in cellular signalling and regulation. *Nat. Rev. Mol. Cell Biol.* **16**, 18–29 (2015).
19. D. Raman, S. Pervaiz, Redox inhibition of protein phosphatase PP2A: Potential implications in oncogenesis and its progression. *Redox Biol.* **27**, 101105 (2019).
20. R. K. Rao, L. W. Clayton, Regulation of protein phosphatase 2A by hydrogen peroxide and glutathionylation. *Biochem. Biophys. Res. Commun.* **293**, 610–616 (2002).
21. J. H. Ahn, M. G. Cho, S. Sohn, J. H. Lee, Inhibition of PP2A activity by H_2O_2 during mitosis disrupts nuclear envelope reassembly and alters nuclear shape. *Exp. Mol. Med.* **51**, 1–18 (2019).
22. Y. C. Kuo, K. Y. Huang, C. H. Yang, Y. S. Yang, W. Y. Lee, C. W. Chiang, Regulation of phosphorylation of Thr-308 of Akt, cell proliferation, and survival by the B55alpha regulatory subunit targeting of the protein phosphatase 2A holoenzyme to Akt. *J. Biol. Chem.* **283**, 1882–1892 (2008).
23. L. L. Coa, T. F. Abreu, A. K. Tashima, J. Green, R. C. Pascon, M. A. Vallim, J. Machado-Jr, AKT/protein kinase B associates with β-actin in the nucleus of melanoma cells. *Biosci. Rep.* **39**, (2019).
24. A. M. Martelli, G. Tabellini, D. Bressanin, A. Ognibene, K. Goto, L. Cocco, C. Evangelisti, The emerging multiple roles of nuclear Akt. *Biochim. Biophys. Acta* **1823**, 2168–2178 (2012).
25. G. Wolff, M. Sakurai, A. Mhamane, M. Troullinaki, A. Maida, I. K. Deligiannis, K. Yin, P. Weber, J. Morgenstern, A. Wieder, Y. Kwon, R. Sekar, A. Zeigerer, M. Roden, M. Blüher, N. Volk, T. Poth, T. Hackert, L. Wiedmann, F. De Angelis Rigotti, J. Rodriguez-Vita, A. Fischer, R. Mukthavaram, P. Limphong, K. Tachikawa, P. Karmali, J. Payne, P. Chivukula, B. Ekim-Üstünel, C. P. Martinez-Jimenez, J. Szendrödi, P. Nawroth, S. Herzig, Hepatocyte-specific activity of TSC22D4 triggers progressive NAFLD by impairing mitochondrial function. *Mol. Metab.* **60**, 101487 (2022).
26. M. Lu, M. Wan, K. F. Leavens, Q. Chu, B. R. Monks, S. Fernandez, R. S. Ahima, K. Ueki, C. R. Kahn, M. J. Birnbaum, Insulin regulates liver metabolism in vivo in the absence of hepatic Akt and Foxo1. *Nat. Med.* **18**, 388–395 (2012).
27. A. Besse-Patin, S. Jeromson, P. Levesque-Damphousse, B. Secco, M. Laplante, J. L. Estall, PGC1A regulates the IRS1:IRS2 ratio during fasting to influence hepatic metabolism downstream of insulin. *Proc. Natl. Acad. Sci. U.S.A.* **116**, 4285–4290 (2019).
28. N. V. Margaritelis, V. Paschalis, A. A. Theodorou, A. Kyparos, M. G. Nikolaidis, Redox basis of exercise physiology. *Redox Biol.* **35**, 101499 (2020).
29. C. Lennicke, H. M. Cocheme, Redox regulation of the insulin signalling pathway. *Redox Biol.* **42**, 101964 (2021).
30. D. H. Kim, D. D. Sarbassov, S. M. Ali, J. E. King, R. R. Latek, H. Erdjument-Bromage, P. Tempst, D. M. Sabatini, mTOR interacts with raptor to form a nutrient-sensitive complex that signals to the cell growth machinery. *Cell* **110**, 163–175 (2002).
31. H. Cho, J. Mu, J. K. Kim, J. L. Thorvaldsen, Q. Chu, E. B. Crenshaw III, K. H. Kaestner, M. S. Bartolomei, G. I. Shulman, M. J. Birnbaum, Insulin resistance and a diabetes mellitus-like syndrome in mice lacking the protein kinase Akt2 (PKB beta). *Science* **292**, 1728–1731 (2001).
32. R. S. Garofalo, S. J. Orena, K. Rafidi, A. J. Torchia, J. L. Stock, A. L. Hildebrandt, T. Coskran, S. C. Black, D. J. Brees, J. R. Wicks, J. D. McNeish, K. G. Coleman, Severe diabetes, age-dependent loss of adipose tissue, and mild growth deficiency in mice lacking Akt2/PKB beta. *J. Clin. Invest.* **112**, 197–208 (2003).
33. B. Dummler, B. A. Hemmings, Physiological roles of PKB/Akt isoforms in development and disease. *Biochem. Soc. Trans.* **35**, 231–235 (2007).
34. P. Narvekar, M. Berriel Diaz, A. Krones-Herzig, U. Hardeland, D. Strzoda, S. Stöhr, M. Frohme, S. Herzig, Liver-specific loss of lipolysis-stimulated lipoprotein receptor triggers systemic hyperlipidemia in mice. *Diabetes* **58**, 1040–1049 (2009).
35. A. J. Rose, M. B. Díaz, A. Reimann, J. Klement, T. Walcher, A. Krones-Herzig, O. Strobel, J. Werner, A. Peters, A. Kleyman, J. P. Tuckermann, A. Vegiopoulos, S. Herzig, Molecular control of systemic bile acid homeostasis by the liver glucocorticoid receptor. *Cell Metab.* **14**, 123–130 (2011).
36. A. Zeigerer, A. Wuttke, G. Marsico, S. Seifert, Y. Kalaidzidis, M. Zerial, Functional properties of hepatocytes in vitro are correlated with cell polarity maintenance. *Exp. Cell Res.* **350**, 242–252 (2017).
37. P. Godoy, N. J. Hewitt, U. Albrecht, M. E. Andersen, N. Ansari, S. Bhattacharya, J. G. Bode, J. Bolleyn, C. Borner, J. Böttger, A. Braeuning, R. A. Budinsky, B. Burkhardt, N. R. Cameron, G. Camussi, C. S. Cho, Y. J. Choi, J. Craig Rowlands, U. Dahmen, G. Damm, O. Dirsch, M. T. Donato, J. Dong, S. Dooley, D. Drasdo, R. Eakins, K. S. Ferreira, V. Fonsato, J. Fraczek, R. Gebhardt, A. Gibson, M. Glanemann, C. E. P. Goldring, M. J. Gómez-Lechón, G. M. M. Groothuis, L. Gustavsson, C. Guyot, D. Hallifax, S. Hammad, A. Hayward, D. Häussinger, C. Hellerbrand, P. Hewitt, S. Hoehme, H. G. Holzhütter, J. B. Houston, J. Hrach, K. Ito, H. Jaeschke, V. Keitel, J. M. Kelm, B. Kevin Park, C. Kordes, G. A. Kullak-Ublick, E. L. LeCluyse, P. Lu, J. Luebke-Wheeler, A. Lutz, D. J. Maltman, M. Matz-Soja, P. McMullen, I. Merfort, S. Messner, C. Meyer, J. Mwinyi, D. J. Naisbitt, A. K. Nussler, P. Olinga, F. Pampaloni, J. Pi, L. Pluta, S. A. Przyborski, A. Ramachandran, V. Rogiers, C. Rowe, C. Schelcher, K. Schmich, M. Schwarz, B. Singh, E. H. K. Stelzer, B. Stieger, R. Stöber, Y. Sugiyama, C. Tetta, W. E. Thasler, T. Vanhaecke, M. Vinken, T. S. Weiss, A. Widera, C. G. Woods, J. J. Xu, K. M. Yarborough, J. G. Hengstler, Recent advances in 2D and 3D in vitro

systems using primary hepatocytes, alternative hepatocyte sources and non-parenchymal liver cells and their use in investigating mechanisms of hepatotoxicity, cell signaling and ADME. *Arch. Toxicol.* **87**, 1315–1530 (2013).
38. L. Buhler, A. Maida, E. S. Vogl, A. Georgiadi, A. Takacs, O. Kluth, A. Schürmann, A. Feuchtinger, C. von Toerne, F.-F. Tsokanos, K. Klepac, G. Wolff, M. Sakurai, B. E. Üstünel, P. Nawroth, S. Herzig, Lipocalin 13 enhances insulin secretion but is dispensable for systemic metabolic control. *Life Sci. Alliance* **4**, e202000898 (2021).
39. S. Herzig, S. Hedrick, I. Morantte, S. H. Koo, F. Galimi, M. Montminy, CREB controls hepatic lipid metabolism through nuclear hormone receptor PPAR-gamma. *Nature* **426**, 190–193 (2003).
40. A. Feuchtinger, T. Stiehler, U. Jütting, G. Marjanovic, B. Luber, R. Langer, A. Walch, Image analysis of immunohistochemistry is superior to visual scoring as shown for patient outcome of esophageal adenocarcinoma. *Histochem. Cell Biol.* **143**, 1–9 (2015).
41. S. Sachs, L. Niu, P. Geyer, S. Jall, M. Kleinert, A. Feuchtinger, K. Stemmer, M. Brielmeier, B. Finan, R. D. DiMarchi, M. H. Tschöp, N. Wewer Albrechtsen, M. Mann, T. D. Müller, S. M. Hofmann, Plasma proteome profiles treatment efficacy of incretin dual agonism in diet-induced obese female and male mice. *Diabetes Obes. Metab.* **23**, 195–207 (2021).

Acknowledgments
Funding: We would like to thank our funding source, German Research Foundation for DFG grants EK 108/1-1 to B.E.Ü. and CRC 1118 to S.H. **Author contributions:** B.E.Ü. conceived and supervised the project. B.E.Ü. and S.D. designed the experiments, performed the experimental work, and did data analysis. G.W. contributed to primary hepatocyte isolation. A.W. and O.H. performed the mouse experiments. M.B. contributed to AV production. A.M. and L.B. contributed to AAV production. A.F. performed the lipid droplet analysis. T.P. performed the H&E staining. J.S. and S.H. contributed to conceptual discussions. B.E.Ü. wrote the manuscript. **Competing interests:** The authors declare that they have no competing interests. **Data and materials availability:** All data needed to evaluate the conclusions in the paper are present in the paper and/or the Supplementary Materials.

Submitted 10 February 2022
Accepted 31 August 2022
Published 21 October 2022
10.1126/sciadv.abo5555